# Design of Artificial Neural Network for predicting the reduction in permeability of porous media as a result of polymer gel injection

Kamel Targhi, Elahe; Emami Niri, Mohammad; L.J. Zitha, Pacelli

**DOI**
10.1016/j.geoen.2023.211925

**Publication date**
2023

**Document Version**
Final published version

**Published in**
Geoenergy Science and Engineering

227 (2023) 211925

Contents lists available at ScienceDirect

Geoenergy Science and Engineering

journal homepage: www.sciencedirect.com/journal/geoenergy-science-and-engineering

# Design of Artificial Neural Network for predicting the reduction in permeability of porous media as a result of polymer gel injection

Elahe Kamel Targhi [a], Mohammad Emami Niri [a,*], Pacelli L.J. Zitha [b]

[a] : Institute of Petroleum Engineering, School of Chemical Engineering, College of Engineering, University of Tehran, Tehran, Iran
[b] : Department of Geoscience and Engineering, Delft University of Technology, Stevinweg 1, Delft, 2628 CN, the Netherlands

ARTICLE INFO

*Keywords:*
Machine Learning
Artificial neural network
Lattice Boltzmann Method
Non-Newtonian fluids
Micro X-ray tomography
CFD
Deep Learning
fluid flow in porous media

ABSTRACT

Cross-linked polymer gel is widely used in the oil and gas industry to block high permeability conduits and reduce water cut. The complex nature of this fluid, especially regarding flow in porous media, makes its numerical simulation very time-consuming. This study presents an approach to designing an Artificial Neural Network (ANN) model that could predict the permeability reduction caused by injecting polymer gel into a 2D rock sample. Our methodology consists of two main parts: numerical simulation and ANN model building. Considering the advantages of the Lattice Boltzmann Method (LBM) this approach is used to model the injection of polymer gel in porous media. Using this model, more than 20,000 simulations were performed which resulted in highly unbalanced dataset, so an innovative approach for balancing regression dataset is also proposed in detail in this paper. The final constructed ANN model could predict the permeability reduction in a fraction of a second with less than 2.5% Mean Absolute Error (MAE). The result indicates the importance of balancing datasets to obtain a reliable prediction from ANN. Also, it should be mentioned that gelation parameters had the most significant impact on the value of permeability reduction, with mean absolute SHapley Additive exPlanations (SHAP) values of 20 and 12.5 for TDfactor and Threshold, respectively.

## 1. Introduction

The undeniable role of nonrenewable energy resources and the low percentage of the recovery factor from oil and gas reservoirs makes it necessary to use suitable Improved Oil Recovery (IOR) and Enhanced Oil Recovery (EOR) methods. Excessive water production is one of the most critical challenges, especially in mature reservoirs (Taha and Amani, 2019). Most studies show that the main reason for the excessive water production is the existence of heterogeneity in high permeability ducts or thief zone (Bai et al., 2015a). Therefore, by blocking high-permeability conduits, the flow paths are changed which subsequently results in producing oil from smaller pores and increasing the sweep efficiency (Dong et al., 2016). Among the existing techniques for reducing water cut, polymer gel has been proven to be the most efficient one (Jiasheng, 2013; Lashari et al., 2014; Liao, 2014; Bai et al., 2015b; Veliyev et al., 2019). Polymer gel can flow through fractures and it is also strong enough to withstand high-pressure differences near the wellbore (Liao, 2014). The mixture of polymer and crosslinker is prepared on the surface and then it is injected through a production well or injection well (Sydansk and Romero-Zerón, 2011). The less viscous solution can penetrate the higher permeability channels and after reaching its gelation time, it will form a solid-like gel that helps the production of oil from unswept regions (Taha and Amani, 2019). Therefore, permeability will be reduced as a result of the injection of polymer gel and the reduction of permeability shows the efficiency of the process.

Although many researchers investigated polymer gel injection experimentally, few attempts have been made to numerically investigate the pore-scale phenomenon associated with the injection of this fluid (Al-Shajalee et al., 2020; Dong et al., 2016; Jia et al., 2011; Zheng et al., 2021; Zitha et al., 2002). Numerical simulations provide researchers with complete control over all parameters that influence pore-scale phenomena and flexibility in modifying and investigating different scenarios and conditions which will be very expensive to do using experiments(Golparvar et al., 2018). Moreover, the high-resolution dataset which is obtained from these methods can be used as a training set for Machine Learning and Deep Learning. Since the polymer is non-Newtonian and time-dependent, it is necessary to choose the best numerical tool for modeling this phenomenon (Parmigiani et al., 2011). Among the available methods, Lattice Boltzmann Method (LBM) has

* Corresponding author.
*E-mail addresses:* kamelelahe@gmail.com (E. Kamel Targhi), emami.m@ut.ac.ir (M. Emami Niri), P.L.J.Zitha@tudelft.nl (P. L.J. Zitha).

https://doi.org/10.1016/j.geoen.2023.211925
Received 6 September 2022; Received in revised form 1 May 2023; Accepted 13 May 2023
Available online 20 May 2023

been proven to have high accuracy and low computational time, especially for complex geometries (Boek and Venturoli, 2010; Martys and Chen, 1996; Olson and Rothman, 1997; Sukop et al., 2008). There are also numerous studies available for simulating non-Newtonian fluid flow with LBM. Different non-Newtonian models such as Carreau-Yasuda (Ashrafizaadeh and Bakhshaei, 2009; Boyd and Buick, 2007; Gokhale and Fernandes, 2017; D. Wang and Bernsdorf, 2009), Carreau (Malaspinas et al., 2007; Yoshino et al., 2007) and Cross (Kehrwald, 2005) have been widely used in the simulation of non-Newtonian fluids with LBM.

Despite the high accuracy of numerical simulation methods, the extensive computational time of these methods has always been a crucial challenge for engineers. Recent developments in artificial intelligence (AI) and machine/deep learning have provided a fantastic tool for predicting the results of simulations and calculations in the shortest possible time. In petroleum engineering, the studies concerned with AI tools can be classified into two general groups: large-scale and small-scale. For large-scale, primary applications of Artificial Neural Networks (ANNs) were limited to well-logging interpretation (Al-Kaabi and Lee, 1993), reservoir characteristics prediction (Mohaghegh and Ameri, 1995; Mohaghegh et al., 1996; Masroor et al., 2022), drilling parameters estimation (Sharifinasab et al., 2023), and formation damage estimation (Nikravesh et al., 1996). Later, the use of AI in this field expanded. Up to this date, many successes have been made in cases such as predicting reservoir properties (i.e., permeability, matrix porosity, and fracture) in dual porosity reservoirs (Alajmi and Ertekin, 2007), history matching for a hydrocarbon field (Haghshenas et al., 2020, 2021; Kolajoobi et al., 2021; Shahkarami et al., 2014), well placement optimization (e.g., Kolajoobi et al., 2023), uncertainty evaluation in reservoir performance prediction (Haddadpour and Emami Niri, 2021), CO2 storage (Van Si and Chon, 2018; Vo Thanh et al., 2020), and Hydrogen Storage (Rahimi et al., 2021).

Unlike large-scale systems that have been studied for years, most of the advances in applying AI-based tools in small-scale studies, particularly in microscopic fields, are related to recent years. Thanks to recent advances in non-destructive imaging technologies, Micro-CT imaging provides a three-dimensional representation of the internal geometry of the porous medium, which can detect pore structures down to several micrometers or even sub-micrometers (Kamrava et al., 2019; Da Wang et al., 2019). This is fascinating data for conducting accurate numerical simulations and using AI techniques. Numerous studies have been conducted on subjects such as image segmentation, reconstruction of porous media, and estimating properties such as porosity, permeability, and resistance factor for a rock sample (Tahmasebi et al., 2020).

Machine learning and deep learning methods have also been recently used to address a variety of problems in fluid mechanics. For example, Hennigh presented a method called Lattice-Network (Lat-Net) to reduce the computation time of LBM (Hennigh, 2017). Lat-Net is an efficient neural network that can be used to reproduce the simulation results of the fluid flow in a porous media. They also showed that when Lat-Net is trained, it can be generalized to large network sizes and complex geometries while maintaining accuracy.

Despite mentioned studies in the field of using AI for fluid flow in porous media and petroleum engineering, there is a significant science gap for the application of machine learning and deep learning for non-Newtonian fluids, especially polymer gel. Moreover, this science gap also exists in predicting the result of polymer gel injection as IOR approach. Since ANNs are proven to learn and recognize problem patterns and explore complex non-linear mathematical relationships between a system's input and output responses, this article presents a novel ANN-based approach to predicting the permeability changes of the two-dimensional porous media after injecting polymer gel. To make the best use of recent advances in the field of imaging porous media, the simulations which were required to build a rich database for training the neural network were done on 2D segmented porous media structure which the details will be discussed in the paper. Providing more than 20,000 combinations of input parameters, numerical simulations are conducted using LBM and permeability reduction is calculated for each case as the most significant parameter to investigate after polymer gel injection. This dataset is then imposed into several stages of data cleaning and reducing the order of the model. Finally, the best ANN is selected by performing several steps of balancing the dataset and selecting the optimum value for hyperparameters. This ANN can predict the changes in the permeability of porous media using the simulation input parameters in a fraction of a second.

In the context of the paper, first, a chapter is specified to LBM background which is required to understand the mathematical model and numerical simulations in this research. Then, in methodology chapter all the steps for numerical simulation and ANN building are discussed in detail and the materials are also provided. The results of all steps are provided in the next chapter and the discussion about the reason behind each of them is done at the same time. The paper is ended up with a conclusion containing some ideas for further works in this area.

## 2. Background

### 2.1. Lattice Boltzmann equation and BGK extension

LBM is selected for modeling the polymer gel injection in porous media in this study. Lattice Boltzmann equation (LBE) is described as:

$$f_i\ (x+e_i,t+1)=f_i(x,t)+\Omega_i(f_i(x,t))(i=1,2\ldots,M) \tag{1}$$

In equation (1) , $f_i$ is distribution function, $e_i$ is discrete velocity, and $\Omega_i$ is collision operator. Since the original collision operator of the Lattice Boltzmann involves all pairwise interactions between molecules, it is necessary to replace it with a simpler one, especially when the problem contains complex phenomenon Therefore, Bhatnagar, Gross, and Krook (BGK) proposed one of the most important and, at the same time, most efficient extensions for collision operators as below (Bhatnagar et al., 1954):

$$\Omega_i(f)=-\frac{1}{\tau}(f_i-f_i^{eq}) \tag{2}$$

Where $f_i^{eq}$ is equilibrium distribution function and $\tau$ is relaxation time. LBGK equation is obtained by replacing equation (2) for collision operator in LBE:

$$f_i(x+e_i,t+1)=f_i(x,t)-\frac{f_i-f_i^{eq}}{\tau} \tag{3}$$

Equation (3) directly considers relaxation towards equilibrium distribution, and transfer coefficients can be obtained easily using the value of τ. For example, the below formula is for kinematic viscosity ($\nu$) (Anbar et al., 2019):

$$\nu=\frac{2\tau-1}{6} \tag{4}$$

### 2.2. Two approaches for implementing non-Newtonian effect in LBM

There are various non-Newtonian models and, in this study, the Carreau model is chosen, which is described as (Ashrafizaadeh and Bakhshaei, 2009; Boyd and Buick, 2007; Gokhale and Fernandes, 2017; D. Wang and Bernsdorf, 2009).:

$$\frac{\nu-\nu_\infty}{\nu_0-\nu_\infty}=\left[1+(\lambda\gamma)^2\right]^{\frac{n-1}{2}} \tag{5}$$

Where $\nu_\infty$ is kinematic viscosity at an infinite shear rate, $\nu_0$ is kinematic viscosity at zero shear rate, λ is the time constant for the fluid, $\gamma$ is the shear rate, and n is the power-law exponent.

Moreover; to the author's knowledge, there are commonly two ways to model a shear-dependent fluid flow in LBM, which will be discussed below.

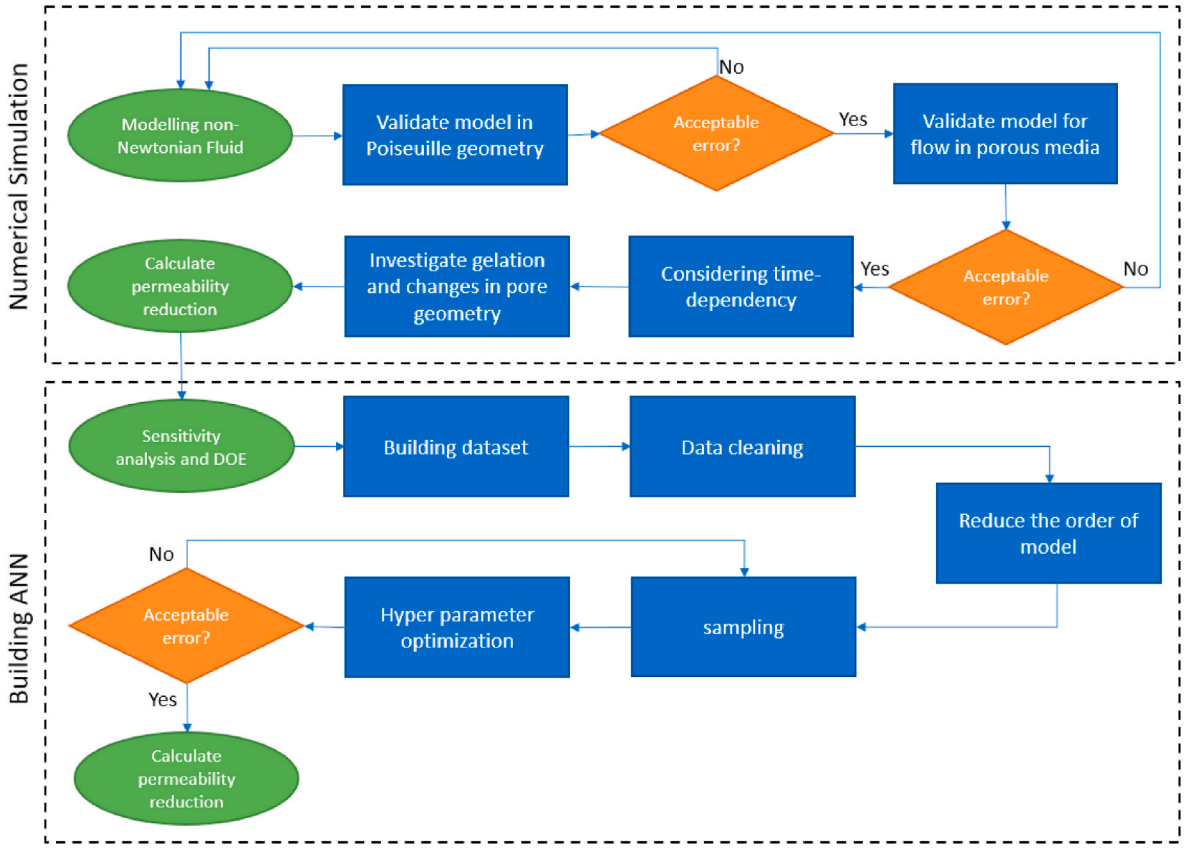


**Fig. 1.** Research methodology.

A) By coupling equations for the kinematic viscosity of the non-Newtonian model and equation (4) shear-dependent relaxation time $\tau$ at each node can be obtained. For the Carreau model, frequency ($\omega$) can be calculated which is the inverse of relaxation time, iteratively, with the below formula (Ohta et al., 2020):

$$\omega = \frac{2}{1 + 2\left(\frac{\nu_0 - \nu_\infty}{c_s^2}\right)\left(1 + \alpha\omega_{iter-1}^2\right)^{\frac{n-1}{2}} + 2\frac{\nu_\infty}{c_s^2}} \tag{6}$$

Where $c_s$ is the sound speed of the lattice, and $\alpha$ is $\frac{1}{2}\frac{\gamma^2}{(\rho c_s^2)^2}$ which $\rho$ is density.

B) Non-Newtonian behavior could also be considered as an equivalent forcing effect. So; it can be say that the non-Newtonian model usually consists of a Newtonian portion and an additional non-Newtonian effect as below (C.-H. Wang and Ho, 2011):

$$f_i(x + e_i, t + 1) = f_i(x, t) - \frac{f_i - f_i^{eq}}{\tau} + \Delta t\left(1 - \frac{\Delta t}{2\tau}\right)\omega_i\left[\frac{e_i - u}{c_s^2} + \frac{(e_i - u)}{c_s^4}\cdot e_i\right]F_{nn} \tag{7}$$

Where $\Delta t$ is the time interval and $F_{nn}$ is a non-Newtonian equivalent forcing effect which can be calculated for different non-Newtonian models.

## 3. Methodology

The methodology for this research is divided into two main stages: numerical simulation and building an ANN model. Fig. 1 summarizes the successive steps of the proposed methodology; details of every step are described hereafter. All of the implementations and codes related to this paper can be found in GitHub repository of the authors.[1]

### 3.1. Numerical simulation

As it is discussed earlier, the aim of this study is to examine the effect of gelation threshold on permeability reduction in a two-dimensional segmented rock image obtained from micro-CT. The numerical simulation stage is divided into smaller steps below to achieve this goal.

1 Modeling non-Newtonian fluid in Palabos:

An open-source software called Palabos (Latt et al., 2021) is selected for numerical simulation. With the help of this software, the flow of Carreau fluid with LBM is modeled. The mathematical model which is used for the simulation is briefly shown in Fig. 2.

2 Validation of model with simulating of non-Newtonian fluid flow in simple geometry (Poiseuille) and comparing the result with the analytical solution:

Before using any CFD code for a real phenomenon, its validity must be checked. Validation ensures that the code accurately solves implemented mathematical models with minimum error. The Poiseuille flow is selected for validation, and the result of the simulation re-checked with an analytical solution as below (Sutera and Skalak, 1993):

$$u(y) = \left(\frac{n}{n+1}\right)\left(\frac{\Delta p}{\rho_{ref}\nu_0}\right)\left[\left(\frac{H}{2}\right)^{\frac{n+1}{n}} - \left(\frac{H}{2} - y\right)^{\frac{n+1}{n}}\right] \tag{8}$$

[1] https://github.com/kamelelahe.

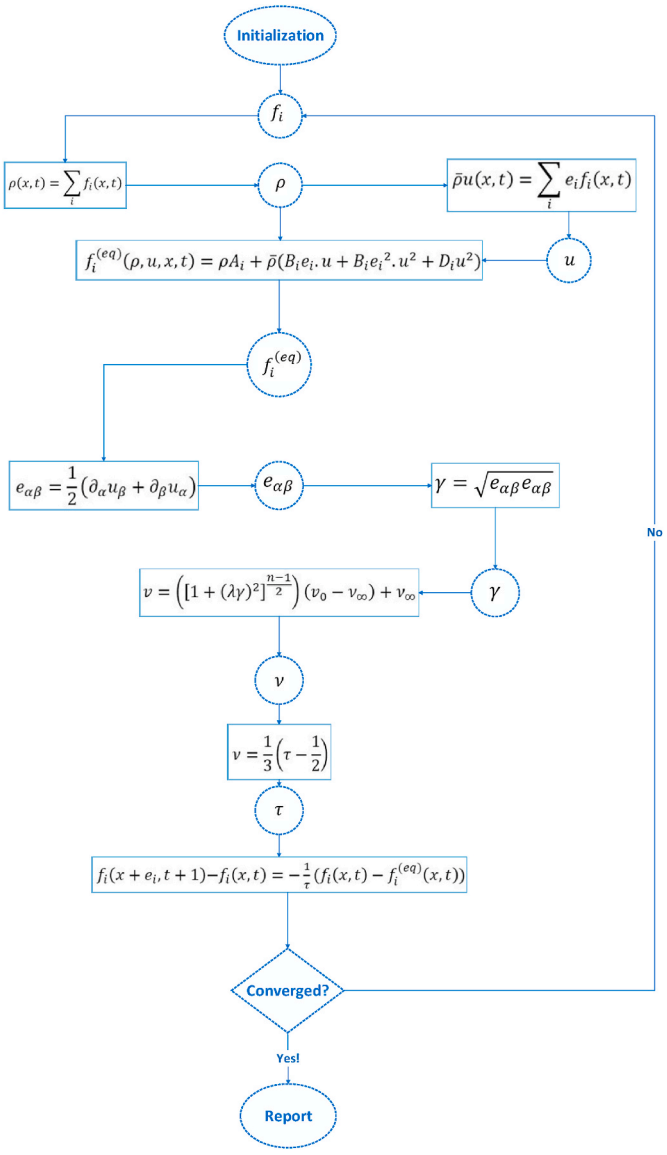


**Fig. 2.** Mathematical methodology for simulating non-Newtonian fluid flow with LBM.

where $u$ is velocity, n is power-law index, $\Delta p$ is pressure difference, $\rho_{ref}$ is reference density, $H$ is the width of the channel or pipe, and $y$ shows the location where the velocity is calculated for that point.

## 3 Validation for fluid flow in porous media

After successfully simulating fluid flow in a simple geometric system, it is necessary to determine if the simulation produces accurate results in more complex systems. To achieve this, the model was first tested for Newtonian fluid flow (n = 1) in a 2D porous media which is obtained from the segmented image of the Berea sandstone micro-model proposed by Boek (Boek and Venturoli, 2010) shown in Fig. 3. The boundary condition in the outlet and inlet is the pressure boundary condition, and the bounce-back scheme is used to model internal boundaries. Next, available analytical solutions and relationships are used to check the accuracy of the model in predicting the behavior of fluid flow in porous media.

## 4 Simulation of polymer gel injection in a porous media:

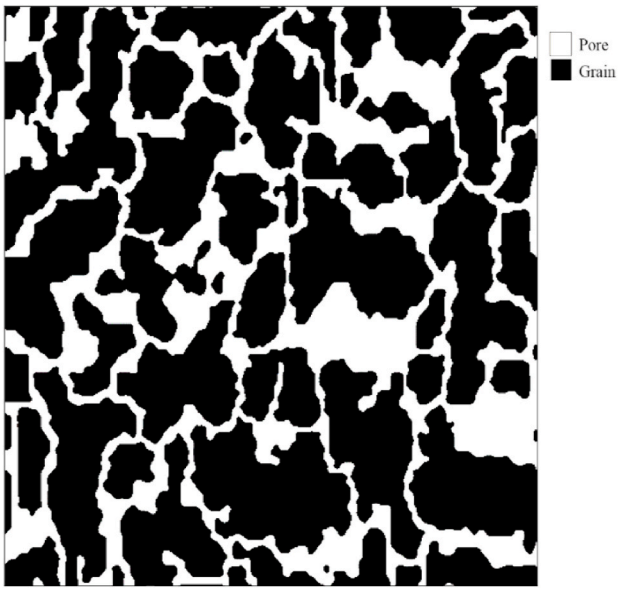


**Fig. 3.** Bera micro model with the size of 1418 μm* 1418 μm, and the etch depth of the physical unit of 24.54 μm. The S pore spaces are in white (Boek and Venturoli, 2010).

Since modeling the injection of polymer gel in porous media can be considered as a combination of two previous steps, after successfully validating those, the model can be confidently used for the problem of this research. The only modification that should be taken into consideration is time dependency because, in fluids such as polymer gel, the viscosity increases over time due to chemical reactions, known as gelation. To model this process, the parameters of the non-Newtonian fluid model must be adjusted after several simulation steps. To simplify this process, the study modeled the gelation process by increasing a parameter called TDfactor, assuming a linear increase in time. This parameter was multiplied in each selected iteration. So, the viscosity increases with time, and the time-thickening behavior of a fluid with the Carreau model is accurately modeled.

## 5 Post-processing and observation of gelation:

In this step, the simulation results should be post-processed to determine the areas where the gel is formed. So, defining a value to describe the highest viscosity in which the fluid can move is required. Since the maximum number for viscosity is infinite, working with the viscosity field is challenging. Hence, relaxation frequency is used which has an inverse relationship with viscosity, and hence a parameter called 'Threshold' is defined to investigate structural changes resulting from gelation. The Threshold is the maximum relaxation frequency at which the fluid can move, and in areas with less relaxation frequency than the Threshold, the formed gel will block pores. Hence, the Threshold value directly affects the permeability change of the porous media after polymer gel injection.

## 6 Investigate changes in the geometry of the porous media and reduction of permeability:

In the next step, gels in the pore structure will be considered rock matrix. So, the final output of this process will show the changes in pore structure after injecting polymer gel. This segmented image can be used to obtain rock properties, i.e., porosity and permeability, and then be compared with the initial values of those properties.

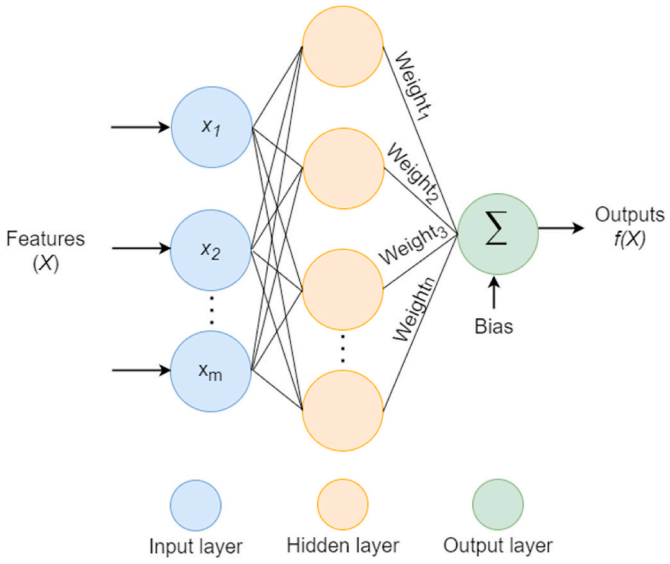


**Fig. 4.** Architecture of artificial neural network.

### 3.2. Building ANN to reduce the computational cost

In the previous section, the key steps of the numerical simulation to calculate the changes in rock structure after injecting polymer gel are described. Since the computational time for numerical methods is too high, numerical simulation for each rock sample may take several hours, and it is necessary to propose some tools/techniques to speed up the process. ANN selected as a powerful tool for this study for two reasons. First, ANN has the ability to learn and model complex nonlinear relationships between input and output data which is useful in fluid flow simulations where the relationship between input parameters and output results can be highly nonlinear and difficult to model using traditional statistical methods. Moreover, ANN can handle large amounts of data with high dimensionality, which is often the case in fluid flow simulations where numerous input parameters and output variables need to be considered. ANN can efficiently learn and represent the underlying patterns and correlations within the data(Rabault et al., 2019; Sen and Yang, 2008).

Therefore, this section describes the steps of constructing a feed-forward to predict permeability changes resulting from polymer gel injection. The architecture of ANN is shown in Fig. 4.

Several steps must be taken to ensure that the built-in AI tool model can correctly predict the target parameter. In the following, most important steps of the model construction process and the necessary concepts in this issue are discussed.

1 Design of Experimental (DOE)

The overall goal of this step is to identify the optimum range for input parameters that can completely cover the range of variations in target parameter/s. For example, this study aims to estimate the permeability changes due to polymer gel injection. DOE helps us propose a set of gelation thresholds and a power-law index for the simulation set on a rock sample that covers all the possible ranges for permeability changes. The required number of samples is not obtained according to a specific relationship, but obviously, it depends on the model's complexity. The more complex the model, the more samples are needed, which ultimately increases the database's size. Careful DOE ensures the comprehensiveness of the final developed model.

2 Database preparation

After performing numerical simulations with the defined model, a dataset should be made with all the information containing input and output values. The database used in this research is a two-dimensional matrix. Since this dataset is the source for training ANN, it must contain the parameters that determine fluid flow characteristics in the porous media and its non-Newtonian behavior. Table 1 shows an overview of the final dataset, which will be used in data mining and cleaning.

3 Data cleaning

Not all simulation data are suitable for network training. The simulations may, in many cases, not converge or show unreasonable values for the output. For example, the output of a simulation may show a negative value for porosity, which is irrational. In the data cleaning stage, the main purpose is to ensure the dataset is free of unnecessary/incorrect simulations.

4 Reduce the order of model (ROM)

The primary database has many features, not all of which may be effective for model training, and their presence dramatically increases the computational volume. Therefore, three main steps are done in ROM to remove any unnecessary features from the dataset.

A. Remove irrelated parameters to the target parameter: The dataset contains many parameters and simulation results, some of which do not help predict target parameters, and removing them is better for computational efficiency.
B. Analysis of distribution functions: After clearing the data, it is time to examine the property distribution functions. Identifying fixed parameters is one of the results of this stage because these parameters, due to constant values, have no effect on the ANN accuracy and are not considered valuable parameters.
C. Identify highly correlated parameters: Since the data is normalized before feeding into ANN, the highly correlated parameters become identical and transfer a series of repetitive patterns. So, in this step, the pairwise correlation between all properties is examined, and among highly correlated parameters, one of them will remain in the final dataset as representative.

5 Sampling

Dealing with an unbalanced dataset is one of the most common and challenging problems for ANN training. In this situation, the distribution function for the target parameter is not uniform. If the network is trained with this dataset, it may provide high numerical accuracy, but it does not give reliable results because the estimated value is more tended to the larger class.

**Table 1**
Overview of the initial dataset.

| | Sample number | Geometric properties | Flow properties | Non-newtonian fluid properties | Gelation parameters | Results |
|---|---|---|---|---|---|---|
| Simulation | 1 | | | | | |
| | 2 | | | | | |
| | 3 | | | | | |
| | … | | | | | |
| | Max. No. of simulation | | | | | |

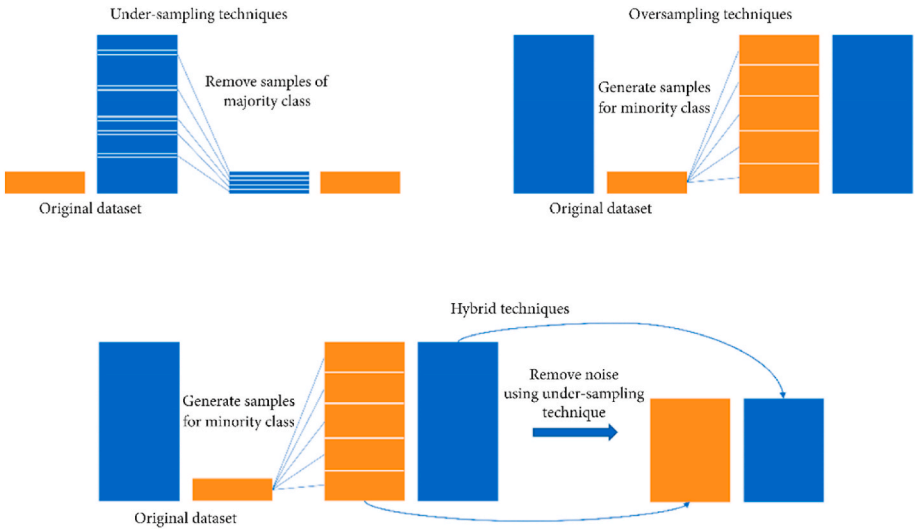


**Fig. 5.** Three common methods for sampling unbalanced data((reproduced from Le et al., 2019).

There are several methods for sampling unbalanced data. Since this situation mainly discusses classification problems, treatments also focus on these kinds of problems. In the following, the top three most common methodologies for sampling are listed. Fig. 5 also summarizes this information graphically.

- Over-sampling: In this method, minority samples are reproduced to increase the number of samples.
- Under-sampling: under-sampling aims to randomly select and remove samples from the majority class, thus reducing the number of samples in the larger class.
- Hybrid technique: This method can overcome the disadvantages of the previous two methods by randomly removing some data from the bigger class and generating random copies of the data in the smaller one.

6 Hyper Parameter Optimization (HPO)

Hyperparameters guide the model's behavior, and their values must be determined before the network training process. The process of selecting the appropriate set of hyperparameters for the learning algorithm is known as HPO. Some of the most critical hyperparameters of ANN are the number of neurons, number of hidden layers, learning rate, and type of activation function. If models in this step fail at this initial assessment in terms of, Mean Absolute Error (MAE), error distribution histogram, and scatter plots, the sampling stage should be repeated to obtain the most accurate results.

7 Model assessment

After successfully constructing ANN, it is time to report the accuracy and performance of the trained network. In addition to the primary measurements done in the previous step, The SHAP Python library is used to analyze the final network with more details (https://github.com/slundberg/shap) to interpret the selected ANN. The SHAP library works by iteratively adding or removing variables in the network and evaluating their relative importance(Lundberg and Lee, 2017).

## 4. Result and discussion

In the previous part of this paper, the methodology of this research was discussed in detail. In this section, the result of this study is also described in two parts, numerical simulation and building an ANN model to reduce computational cost.

**Table 2**
Input parameters for Poiseuille flow of Carreau fluid.

| Parameter | Value |
|---|---|
| u | 0.004951 |
| Re | 1 |
| Cu | 10 |
| N | 101 |
| lx | 1.00E+00 |
| ly | 1 |
| lz | 0.00E+00 |
| dx | 0.009901 |
| dt | 4.90E-05 |
| n | 0.5 |
| nu0 | 5.00E-01 |
| nuInf | 0 |
| omega0 | 0.5 |
| omegaInf | 2 |
| lambda | 204020 |

### 4.1. Numerical simulation

#### 4.1.1. Model validation of non-Newtonian fluid flow in simple geometry (Poiseuille)

As discussed in the previous section, it is necessary to check the model's validity in simple geometry before using it for more complex phenomena. An analytical solution was introduced for the velocity distribution of Poiseuille flow of non-Newtonian fluid in eq. (1). Here, we checked our code for Poiseuille flow with the properties listed in Table 2 and compared the result with the numerical solution. As is shown in Fig. 6, the model could perfectly catch the behavior of non-Newtonian fluid in this problem.

#### 4.1.2. Verify the code for the flow of Newtonian fluid in porous media

Porous media geometry is very complex, so it is necessary to check if the model can capture the flow properties in this geometry. Since, in contrast to Poiseuille flow, there is no analytical solution for the flow of non-Newtonian fluid in porous media, the best possible way is to check whether this model agrees with Darcy's law which is stated in eq. (7) as below:

$$u = -\frac{k}{\mu}\frac{\Delta p}{l} \tag{9}$$

Where u is velocity, k is permeability, $\mu$ is viscosity, $\Delta p$ is pressure difference, and $l$ is the length of the flow domain. Since Darcy's law is

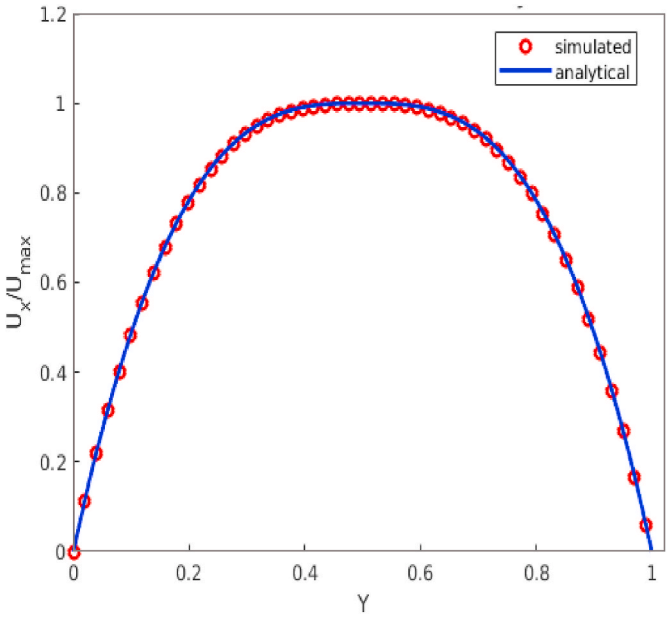


**Fig. 6.** Comparing the simulation result and analytical solution for normalized velocity profile of Poiseuille flow of non-Newtonian fluid of Table 1. The comparison shows an excellent match.

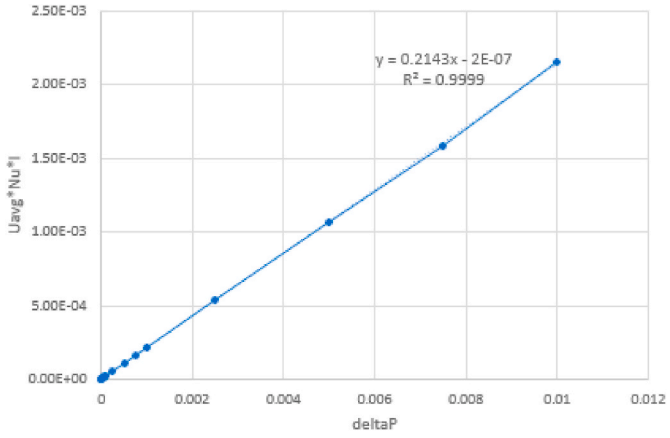


**Fig. 7.** Validation of flow of Newtonian fluid in 2D Berea sample. The slope of this plot indicates permeability.

only valid for Newtonian fluid, for this fluid, it should be a linear relationship between velocity and $\frac{\Delta p}{\mu * l}$. So, to check this relationship for the proposed model, the simulation parameters set to n = 1 and TDfactor = 1 to consider the Newtonian behavior of fluid flowing in the Berea sample (Fig. 3). Then numerous simulations are conducted by changing $\Delta p$ and keeping other parameters constant. The boundary conditions are constant pressure (Zou and He) at the inlet and outlet (right and left side) and the bounce-back scheme applied in the rock and fluid domain interface. As it is shown in Fig. 7, our model could successfully capture the linear relationship between u and $\frac{\Delta p}{\mu * l}$. Also, the slope of this plot is 0.214, which agrees with the code's estimated permeability.

### 4.1.3. Simulation of polymer injection in porous media

After conducting two validation parts, the model can be used confidently for simulating the injection of polymer-gel in porous media. In this section, the result for the step 4–6 in numerical simulation (which is discussed in section 4.1) is provided. The flow of three different types of fluids, i.e., Newtonian fluid, polymer (shear-thinning), and polymer gel (shear-thinning and time-thickening), is simulated in Berea geometry. User input parameters for this code are Nx (number of lattices in the horizontal direction), Ny (number of lattices in the vertical direction), deltaP (pressure difference), n(power-law index), Nu0 (viscosity at zero shear rate), Cu (Carreau number), TDfactor (refer to step 4 section 4.1and Threshold(refer to step 5 section 4.1). All input parameters (user-defined and simulator defaults) and the results of these simulations are presented in Table 3 and the units are provided in parentheses.

As shown in Fig. 8, the omega field for Newtonian fluid has a constant value everywhere in the domain, which agrees with the nature of Newtonian fluids, which are shear-independent.On the other hand, omega shows higher values in smaller pores with higher velocity or shear rate for the two other types of fluid and shows the shear-thinning behavior of the fluid. Also, comparing the rock geometries at the end of

**Table 3**
Simulation parameters and results of Newtonian, time-independent non-Newtonian, and time-dependent non-Newtonian fluids' motions in a 2D Berea sample.

| | # | Parameter | Newtonian | polymer | Polymer gel |
|---|---|---|---|---|---|
| Porous media properties | 1 | N | 400 | 400 | 400 |
| | 2 | lx | 1 | 1 | 1 |
| | 3 | ly | 1 | 1 | 1 |
| | 4 | lz | 0 | 0 | 0 |
| | 5 | Dx (LU) | 0.0025 | 0.0025 | 0.0025 |
| | 6 | Dt (TS) | 1.54E-07 | 1.54E-07 | 1.54E-07 |
| | 7 | Nx | 400 | 400 | 400 |
| | 8 | Ny | 400 | 400 | 400 |
| Flow properties | 9 | U ($\frac{LU}{TS}$) | 6.15E-05 | 6.15E-05 | 6.15E-05 |
| | 10 | Re | 0.12 | 0.12 | 0.12 |
| | 11 | deltaP ($\frac{MU \times LU}{TS^2}$) | 0.0005 | 0.0005 | 0.0005 |
| Non-Newtonian fluid properties | 12 | Cu | 5 | 5 | 5 |
| | 13 | n | 1 | 0.8 | 0.8 |
| | 14 | Nu0 ($\frac{LU^2}{TS}$) | 0.2 | 0.2 | 0.2 |
| | 15 | NuInf ($\frac{LU^2}{TS}$) | 0 | 0 | 0 |
| | 16 | Omega0 | 0.91 | 0.91 | 0.91 |
| | 17 | OmegaInf | 2 | 2 | 2 |
| | 18 | lambda | 3.25E+07 | 3.25E+07 | 3.25E+07 |
| Gelation parameters | 19 | threshold | 0.75 | 0.75 | 0.75 |
| | 20 | TDfactor | 1 | 1 | 1.11 |
| Results | 21 | AvgNu ($\frac{LU^2}{TS}$) | 0.93 | 0.62 | 1.08 |
| | 22 | AvgOmega | 0.30 | 0.42 | 0.27 |
| | 23 | AvgVel ($\frac{LU}{TS}$) | 0.00 | 0.00 | 0.00 |
| | 24 | AvgP ($\frac{MU \times LU}{TS^2}$) | 1.00 | 1.00 | 1.00 |
| | 25 | GradP ($\frac{MU \times LU}{TS^2}$) | 0.00 | 0.00 | 0.00 |
| | 26 | qNorm ($\frac{LU^3}{TS}$) | 0.00 | 0.00 | 0.00 |
| | 27 | MaxShear ($\frac{1}{TS}$) | 0.00 | 0.00 | 0.00 |
| | 28 | MinShear ($\frac{1}{TS}$) | 0 | 0 | 0 |
| | 29 | MaxOmega | 0.91 | 1.67 | 1.27 |
| | 30 | MinOmega | 0 | 0 | 0 |
| | 31 | MaxVel ($\frac{LU}{TS}$) | 0.00 | 0.00 | 0.00 |
| | 32 | MinVel ($\frac{LU}{TS}$) | 0 | 0 | 0 |
| | 33 | porosity | 0.33 | 0.33 | 0.20 |
| | 34 | Perm ($LU^2$) | 0.21 | 0.21 | 0.02 |
| | 35 | poroPerc (%) | 0 | 0 | 45.12 |
| | 36 | permPerc (%) | 0 | 0 | 93.43 |

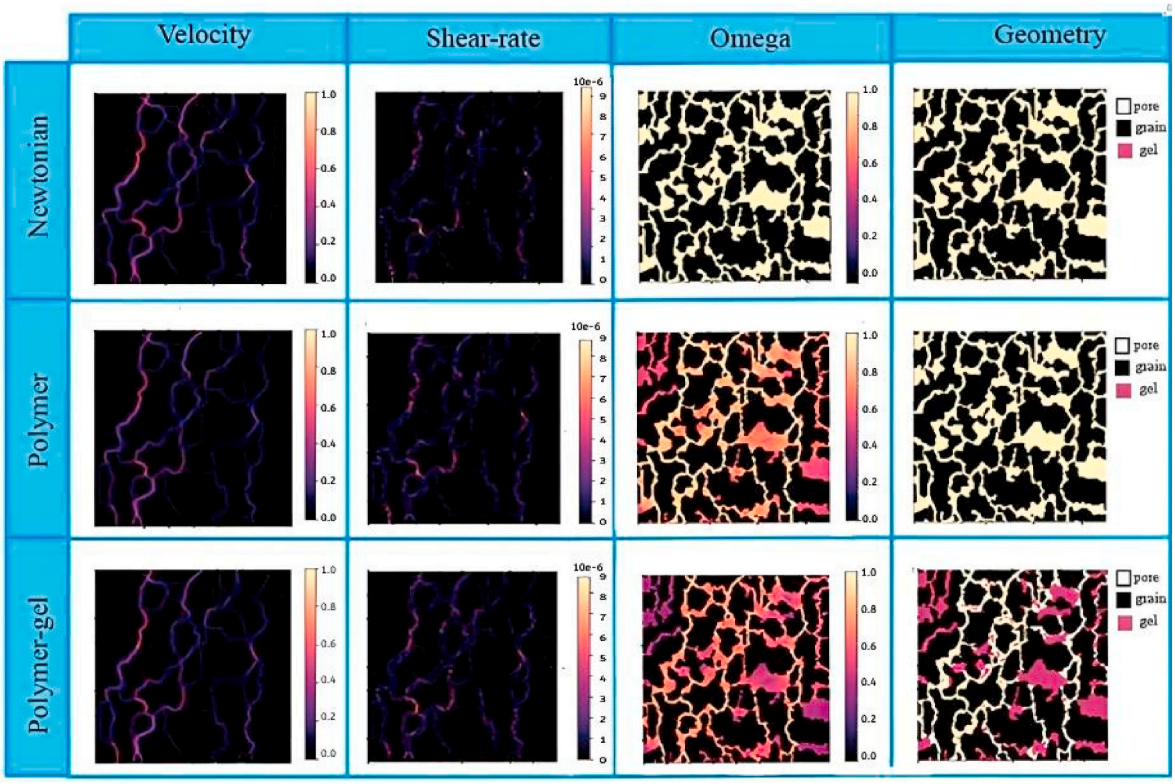


**Fig. 8.** Velocity field, shear rate, omega, and geometry changes after injecting different types of fluids in a 2D Berea sample.

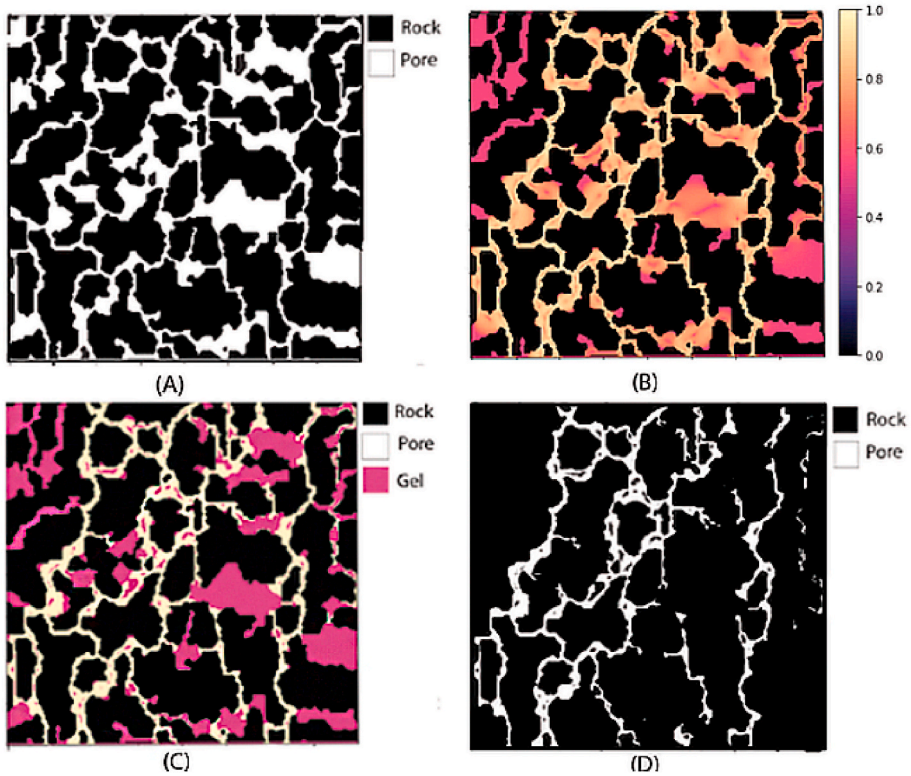


**Fig. 9.** Schematic of different stages of the simulation. (A)initial rock geometry, (B)relaxation frequency field at the end simulation, (C)formation of gel in pores, (D) rock geometry after injection of polymer gel.

**Table 4**
Range of input parameters for numerical simulation.

| Parameter | Initially selected range | Optimum range |
|---|---|---|
| deltaP | {1e-5,5e-5,1e-4,5e-4,0.001,0.005,0.01} | {1e-5,5e-5,1e-4,5e-4,0.001,0.005} |
| Nu0 | {0.1,0.2,0.3,0.4,0.5,0.6,0.7,0.8} | {0.2,0.3,0.4,0.5,0.6,0.7,0.8} |
| n | {0.3,0.4,0.5,0.6,0.7,0.8,0.9,1} | {0.5,0.6,0.7,0.8,0.9,1} |
| Cu | {1,5,10,15,20} | {1,5,10,15} |

the simulation reveals that this model could successfully capture the formation of gel in pores, and gel is mainly formed in larger pores. Since the ultimate goal in injecting polymer gel is to block the high permeable paths and improve oil displacement from narrower conduits, it seems could the model is able to successfully capture the behavior of the phenomenon.

To take a closer look, in Fig. 9, the simulation procedure stages for polymer gel injection are shown. As it could be clearly understood from this figure, the changes in pore geometry are carefully captured by the proposed numerical model.

### 4.2. Building an ANN model to reduce the computational cost

After successfully simulating the phenomenon, it is time to use it in building a rich database and make the database ready for building an efficient ANN. The results of the steps in this procedure are gathered in this section.

#### 4.2.1. Sensitivity analysis and DOE

The first step in building an ANN is to prepare a good database that covers all the possibilities and optimum ranges for each parameter. Therefore, 2240 simulations were performed with input parameters from Table 4 to select their optimal values for numerical simulation. Then, a pairwise sensitivity analysis is carried out on generated simulation results to identify the input parameters with a higher risk of divergence. Fig. 10 shows the percentage of simulation divergence for each pair of input parameters in which brighter blocks have a higher risk of divergence. As can be seen from the images in Fig. 10, the simulations with low values of n and Nu0 and high values of the pressure difference and Cu have a higher chance of diverging. As a result of this step, the optimum range for simulation input parameters is obtained and reported in Table 4.

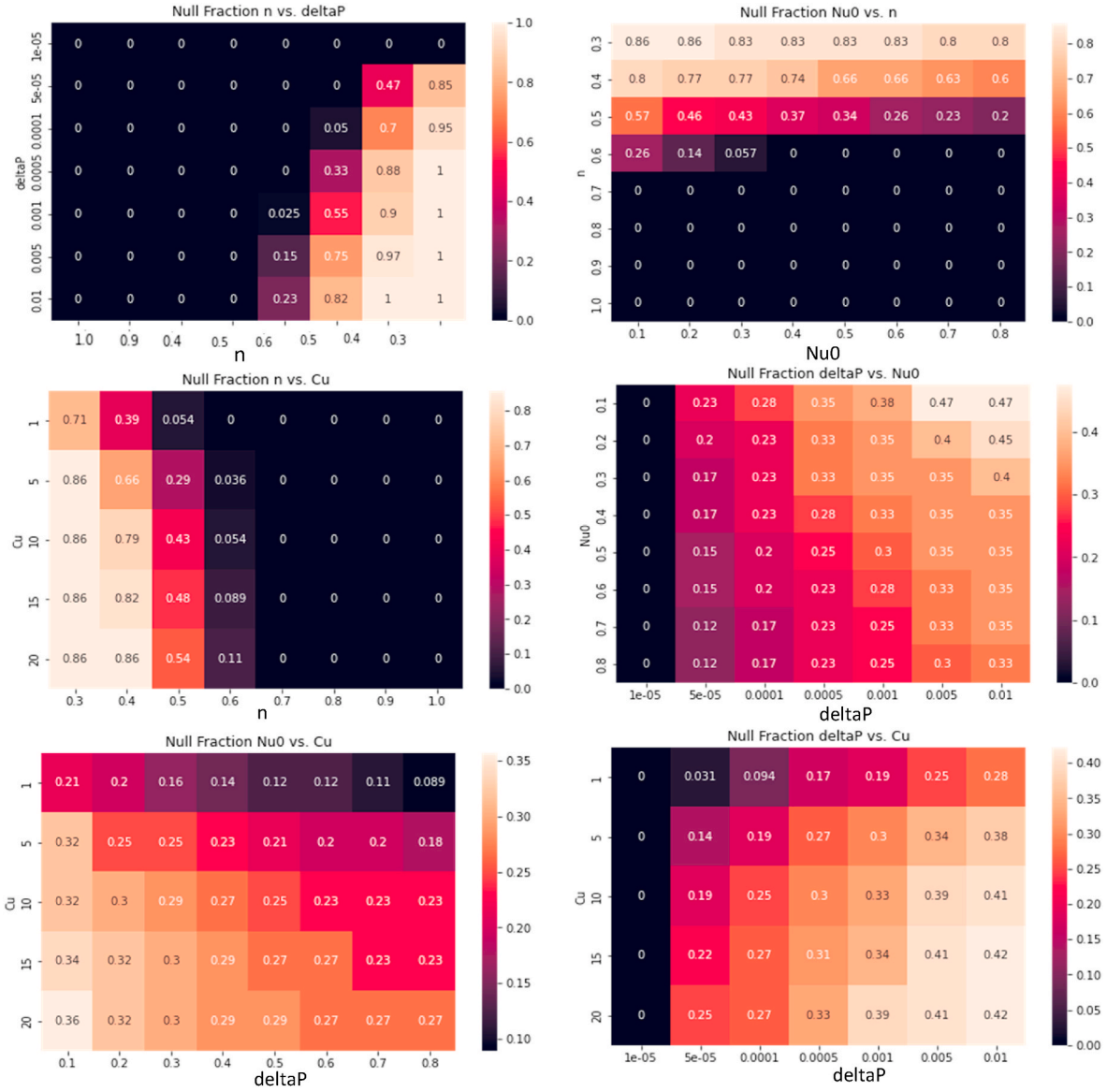


**Fig. 10.** Pairwise sensitivity analysis on the divergence of simulation results.

**Table 5**
Values for input parameters in building initial dataset.

| Parameter | Selected values | Count |
|---|---|---|
| deltaP | {1e-5,5e-5,1e-4,5e-4,0.001,0.005} | 6 |
| Cu | {5,7,10,12,15} | 5 |
| n | {0.5,0.6,0.7,0.8,0.9,1} | 6 |
| TDfactor | {1,1.01,1.02,1.03,1.04,1.05,1.06,1.07,1.08,1.09,1.1,1.11,1.12,1.13,1.14,1.15} | 16 |
| Threshold | {0.6,0.65,0.7,0.75,0.8,0.85,0.9} | 7 |
| Total number of simulations: 20160 = 6*5*6*16*7 | | |

**Table 6**
Overview of the initial dataset.

| | 1 | RunNum | 1 | 2 | 3 | … | 20160 |
|---|---|---|---|---|---|---|---|
| Geometrical properties | 2 | N | 400 | 400 | 400 | … | 400 |
| | 3 | lx | 1 | 1 | 1 | … | 1 |
| | 4 | ly | 1 | 1 | 1 | … | 1 |
| | 5 | lz | 0 | 0 | 0 | … | 0 |
| | 6 | dx | 0.0025 | 0.0025 | 0.0025 | … | 0.0025 |
| | 7 | dt | 1.55E-06 | 3.08E-07 | 1.54E-07 | … | 3.07E-09 |
| | 8 | Nx | 400 | 400 | 400 | … | 400 |
| | 9 | Ny | 400 | 400 | 400 | … | 400 |
| Flow properties | 10 | u | 0.000621 | 0.000123 | 6.15E-05 | … | 1.23E-06 |
| | 11 | Re | 1.24227 | 0.246121 | 0.122916 | … | 0.002456 |
| | 12 | deltaP | 0.005 | 0.001 | 0.0005 | … | 0.00001 |
| Non-newtonian fluid properties | 13 | Cu | 5 | 5 | 5 | … | 15 |
| | 14 | n | 1 | 1 | 1 | … | 0.5 |
| | 15 | Nu0 | 0.2 | 0.2 | 0.2 | … | 0.2 |
| | 16 | NuInf | 0 | 0 | 0 | … | 0 |
| | 17 | OmegaO | 0.909091 | 0.909091 | 0.909091 | … | 0.909091 |
| | 18 | OmegaInf | 2 | 2 | 2 | … | 2 |
| | 19 | lambda | 3219900 | 16252200 | 32542500 | … | 4.89E+09 |
| Gelation parameters | 20 | threshold | 0.9 | 0.9 | 0.9 | … | 1.15 |
| | 21 | TDfactor | 1 | 1 | 1 | … | 0.492378 |
| Results | 22 | AvgNu | 0.934662 | 0.934662 | 0.934662 | … | 0.505783 |
| | 23 | AvgOmega | 0.302665 | 0.302665 | 0.302665 | … | 2.12E-06 |
| | 24 | AvgVelTotal | 1.36E-05 | 2.71E-06 | 1.35E-06 | … | 0.332927 |
| | 25 | AvgDen | 0.330785 | 0.332502 | 0.332717 | … | 0.998781 |
| | 26 | AvgP | 0.992356 | 0.997506 | 0.99815 | … | 2.51E-08 |
| | 27 | GradP | 1.25E-05 | 2.51E-06 | 1.25E-06 | … | 0.000856 |
| | 28 | qNorm | 0.005317 | 0.001051 | 0.000525 | … | 1.41E-07 |
| | 29 | MaxShear | 0.000105 | 0.000021 | 1.05E-05 | … | 0 |
| | 30 | MinShear | 0 | 0 | 0 | … | 1.99062 |
| | 31 | MaxOmega | 0.909091 | 0.909091 | 0.909091 | … | 0 |
| | 32 | MinOmega | 0 | 0 | 0 | … | 0.000159 |
| | 33 | MaxVel | 0.000646 | 0.000128 | 0.000064 | … | 0 |
| | 34 | MinVel | 0 | 0 | 0 | … | 0.9 |
| | 35 | porosity | 0.332931 | 0.332931 | 0.332931 | … | 0.259944 |
| | 36 | perm | 0.214527 | 0.214527 | 0.214527 | … | 4619.59 |
| | 37 | poroPerc | 0 | 0 | 0 | … | 21.92269 |
| | 38 | permPerc | 0 | 0 | 0 | … | −2153284 |

#### 4.2.2. Building dataset

After selecting the optimum range of values for the simulation parameters, it is time to build the database. Up to this purpose, 20160 simulations were run with those values of input parameters listed in Table 5. Table 6 depicts an overview of the initial database, and the table is transposed to be easier to read.

#### 4.2.3. Data cleaning

As discussed, the initial dataset contains 20160 rows (number of simulations performed) and 38 columns (total number of parameters). For data cleaning, firstly, rows containing NaN for simulation results were removed, then irrational data such as rows with porosity values greater than one or negative and rows with zero value for permeability were eliminated. After this step, the size of the database is reduced to 38 * 14847, which means that 5313 rows have been removed from it.

#### 4.2.4. ROM

The next step is to reduce the number of parameters in the dataset. First, unrelated parameters (such as average viscosity and maximum shear rate) to the target parameter (permeability reduction (are removed. By doing this, 14 features (rows 22 to 36 in Table 6) are eliminated from the database, and its dimensions are reduced to 14847 * 24.

Next, the distribution plots are examined to identify parameters with constant values in all simulations and remove them from the database. As shown in Fig. 11, for example, the parameters related to the simulation dimensions are consistent for all simulations. So N, lx, ly, lz, dx, Nx, Ny, Nu0, NuInf, Omega0, and OmegaInf are removed from the dataset, and the dimension of the dataset is reduced to 14847 * 13.

As a final step in ROM, the linear correlation between the remaining parameters in the database is examined. One parameter is selected as a representative one with a high linear correlation. In Fig. 12, a heatmap is used to represent the value for correlation graphically. As a result of this step, dt, u, Re, porosity, and perm are removed from the database, and the database dimension is reduced to 14847 * 8.

Fig. 13 summarizes data cleaning and ROM steps which were described in detail in this section. It could be seen that more than 5000 simulations (almost one-third of the dataset) were removed at this stage,

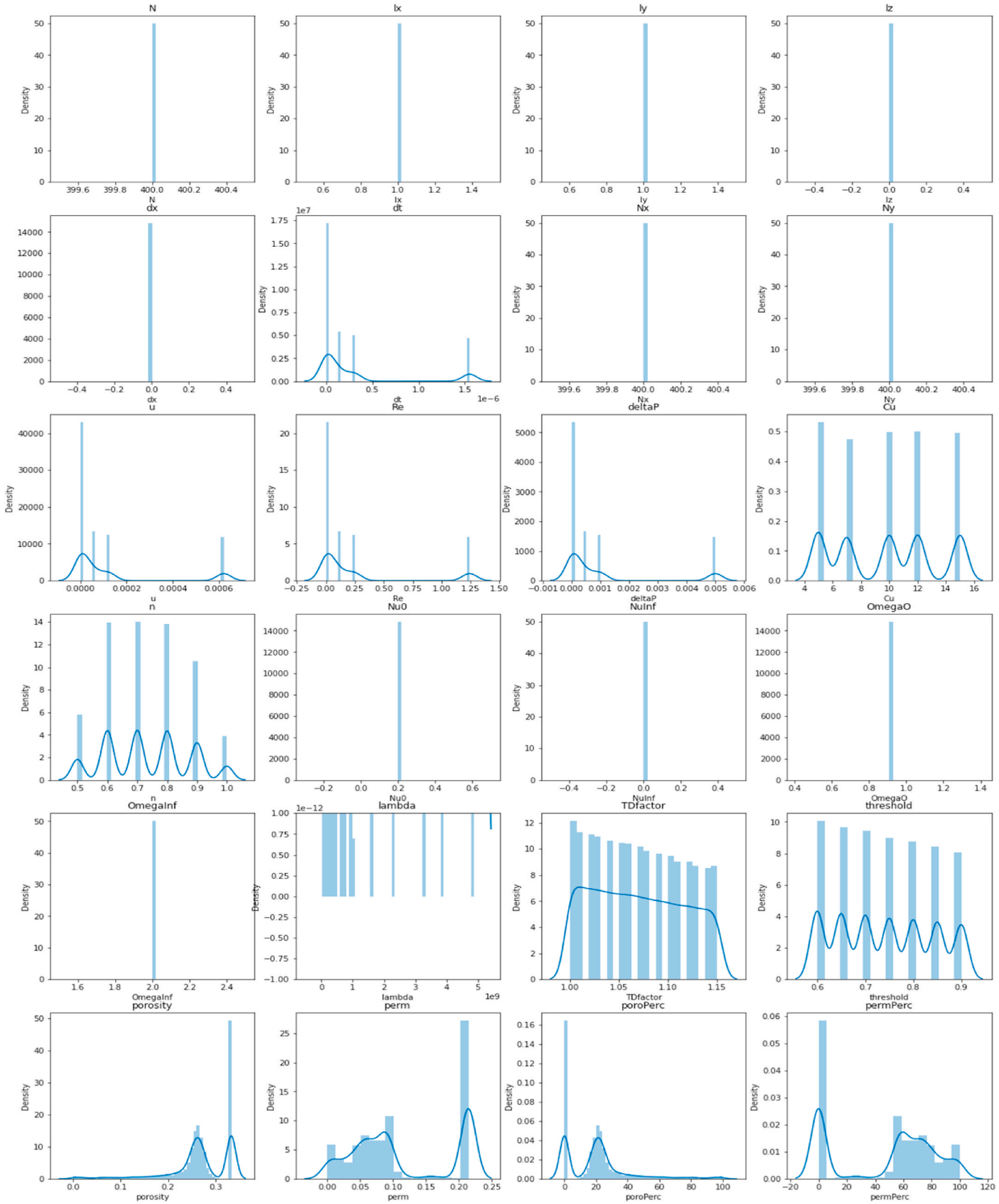


**Fig. 11.** Distribution diagrams of different simulation parameters.

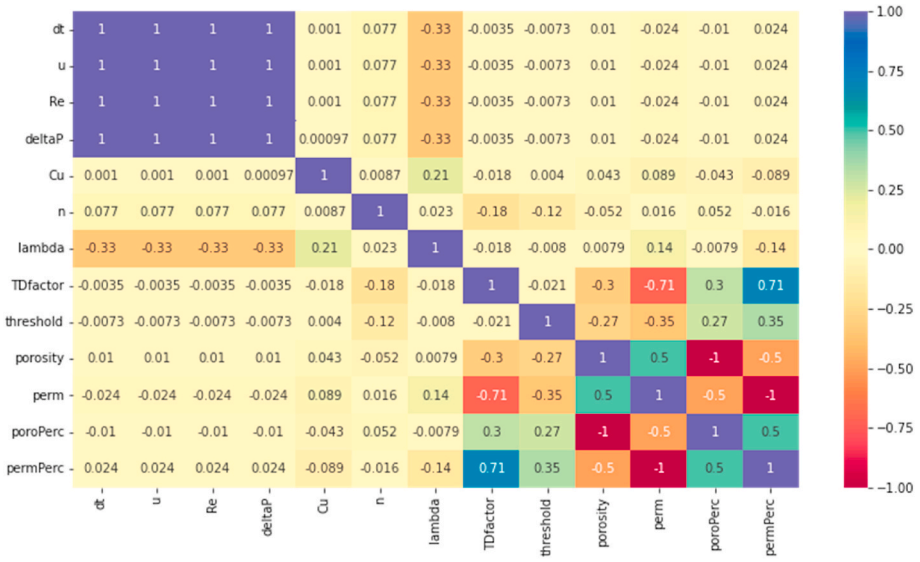


**Fig. 12.** Heat map for pairwise linear correlation between available parameters.

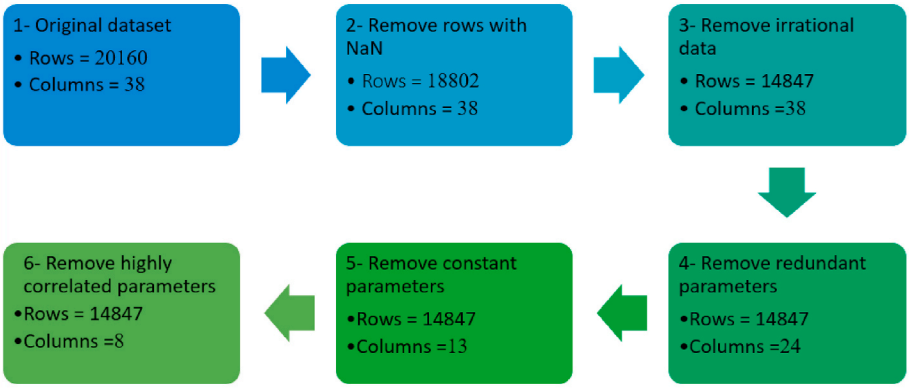


**Fig. 13.** Dimension of the dataset in every step of data cleaning and ROM.

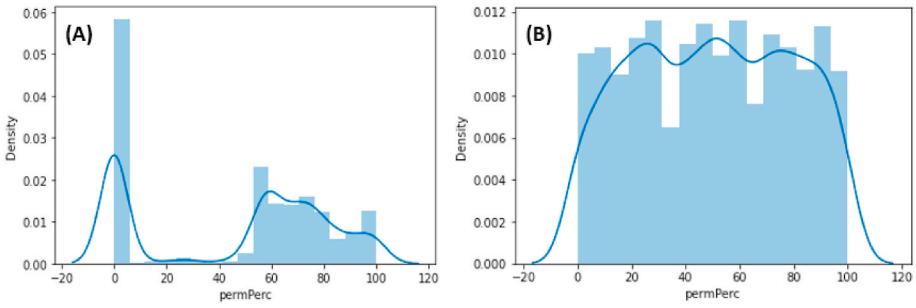


**Fig. 14.** Density plot for target parameter A) before balancing, B) after the first balancing step.

and also, the number of parameters decreased from 38 to 8, which means only less than 20% of simulation parameters were useful for training ANN.

*4.2.5. Sampling- 1st step*

Initial analysis of the target parameter density plot (Fig. 14(A)) shows that the dataset for this study is highly unbalanced. For a large proportion of the simulation, there were no changes in permeability, meaning the fluid did not reach the gelation criteria due to several reasons, including missing non-Newtonian characteristics, low values for TDfactor, and high values for Threshold. As discussed in the previous section, although the network trained with this data may have good accuracy, it is unreliable, and its predictions are biased toward zero values for permeability reduction.

This study uses a combination of over-sampling and under-sampling methods to balance the database. Since the research problem is regression, dividing the permeability reduction percentage into different classes before sampling is necessary. Therefore, the data is divided into 20 different classes based on the percentage of permeability reduction, and then 200 samples from each category are selected for network

**Table 7**
Specifications of the models used in the first step selecting the number of hidden layers and neurons.

| MODEL NUMBER | 1 | 2 | 3 | 4 | 5 | 6 | 7 | 8 | 9 | 10 | 11 | 12 |
|---|---|---|---|---|---|---|---|---|---|---|---|---|
| NO. OF INPUT PARAMETERS | 6 | 6 | 6 | 6 | 6 | 6 | 6 | 6 | 6 | 6 | 6 | 6 |
| NO. OF HIDDEN LAYERS | 1 | 2 | 3 | 4 | 1 | 2 | 3 | 4 | 1 | 2 | 3 | 4 |
| NO. OF NEURONS | 11 | 11 | 11 | 11 | 15 | 15 | 15 | 15 | 19 | 19 | 19 | 19 |
| ACTIVATION FUNCTION | ReLU | ReLU | ReLU | ReLU | ReLU | ReLU | ReLU | ReLU | ReLU | Relu | Relu | Relu |
| TRAINING ALGORITHM | Adam | Adam | Adam | Adam | Adam | Adam | Adam | Adam | Adam | Adam | Adam | Adam |
| LEARNING RATE | 0.001 | 0.001 | 0.001 | 0.001 | 0.001 | 0.001 | 0.001 | 0.001 | 0.001 | 0.001 | 0.001 | 0.001 |

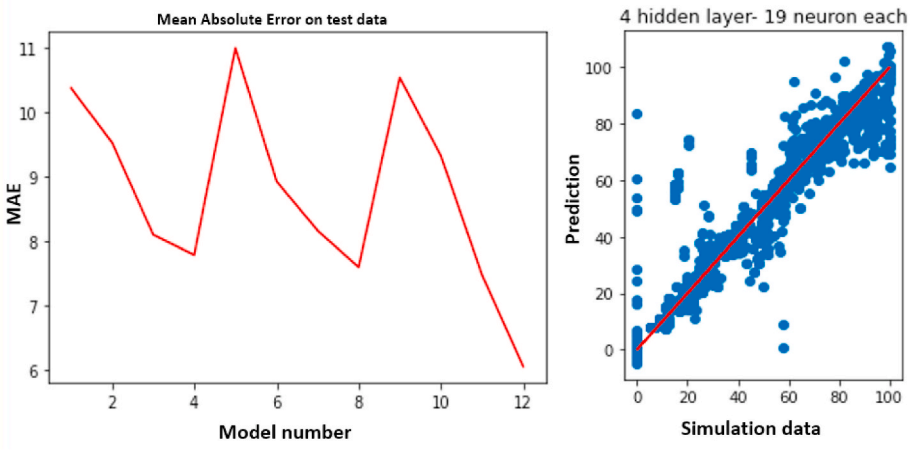


**Fig. 15.** Simulation Error for Models with Different Layers and Neurons and scatter plot for the selected network (model no. 12).

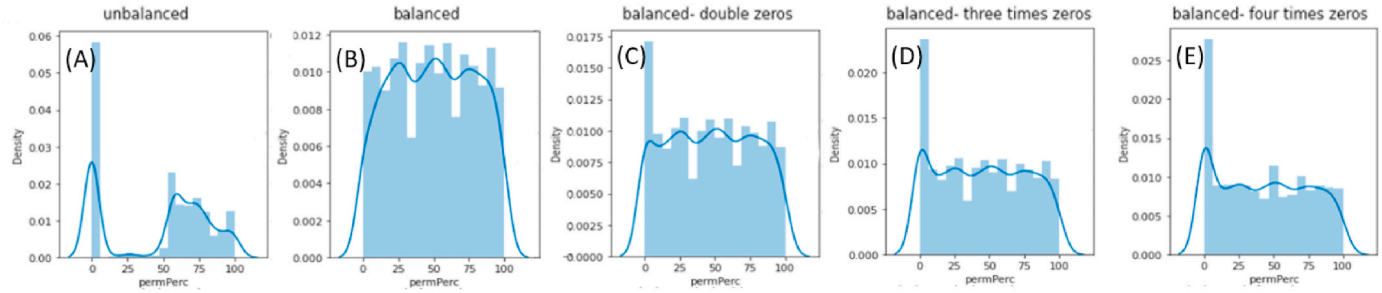


**Fig. 16.** Target parameter distribution in the unbalanced dataset (1), balanced dataset(2), increasing row with zero permeability reduction 2, 3, and 4 times (datasets no 3, 4, and 5, respectively).

training. Fig. 14(B) shows the distribution of the percentage of permeability reduction after base balancing.

### 4.2.6. *HPO- 1st step*

Optimum values for hyperparameters in this study are selected with trial and error. Twelve ANNs were trained at the first step, and their characteristics are summarized in Table 7. For all the ANNs implemented in this study, train_test_split function from scikit-learn library is used to split the dataset, and 30% of data are randomly used for test and the rest are for training. As is shown in Fig. 15, MAE for model no.12, with 4 layers and 19 neurons in each layer, has the minimum MAE. Also, the scatter plot of simulation results versus the predicted value shows that it is the most suitable ANN for predicting permeability reduction.

*4.2.6.1. Sampling- 2nd step.* Although the MAE for model number 12 is less than 7%, the presence of a vertical line in predicting simulations with zero permeability reduction motivates us to build a better ANN. As discussed in the methodology step, sampling should be repeated. This time, the number of data with zero permeability reduction in the balanced database has increased 2, 3, and 4 times. The distribution plot of the target parameter in these datasets is shown in Fig. 16.

Then these datasets are used for training networks with the same characteristics as model number 12 in Table 7 (4 hidden layers, 19 neurons per layer, and a learning rate of 0.001). As shown in Fig. 17, for dataset number 5, the scatter plot shows better prediction, and the error distribution plot is also more normal. So this dataset is selected for further analysis.

### 4.2.7. *HPO- 2nd step*

After selecting the potential dataset, the HPO step must be repeated to achieve better accuracy. Since the proposed ANN has six input parameters, increasing the number of neurons to more than 19 does not help us improve the accuracy. So the number of neurons in each layer is kept 19 and different numbers of hidden layers (1–8) are selected to train ANNs. The characteristics of these ANNs are available in Table 8. As shown in Fig. 18, model number 7 has a better estimation and less MAE.

Although the error for model number 7 in Table 8 is less than 5 percent, the scatter plot shows us that ANN still does not have good accuracy in predicting simulation results with zero permeability. As the second hyperparameter to optimize in this step, the learning rate should

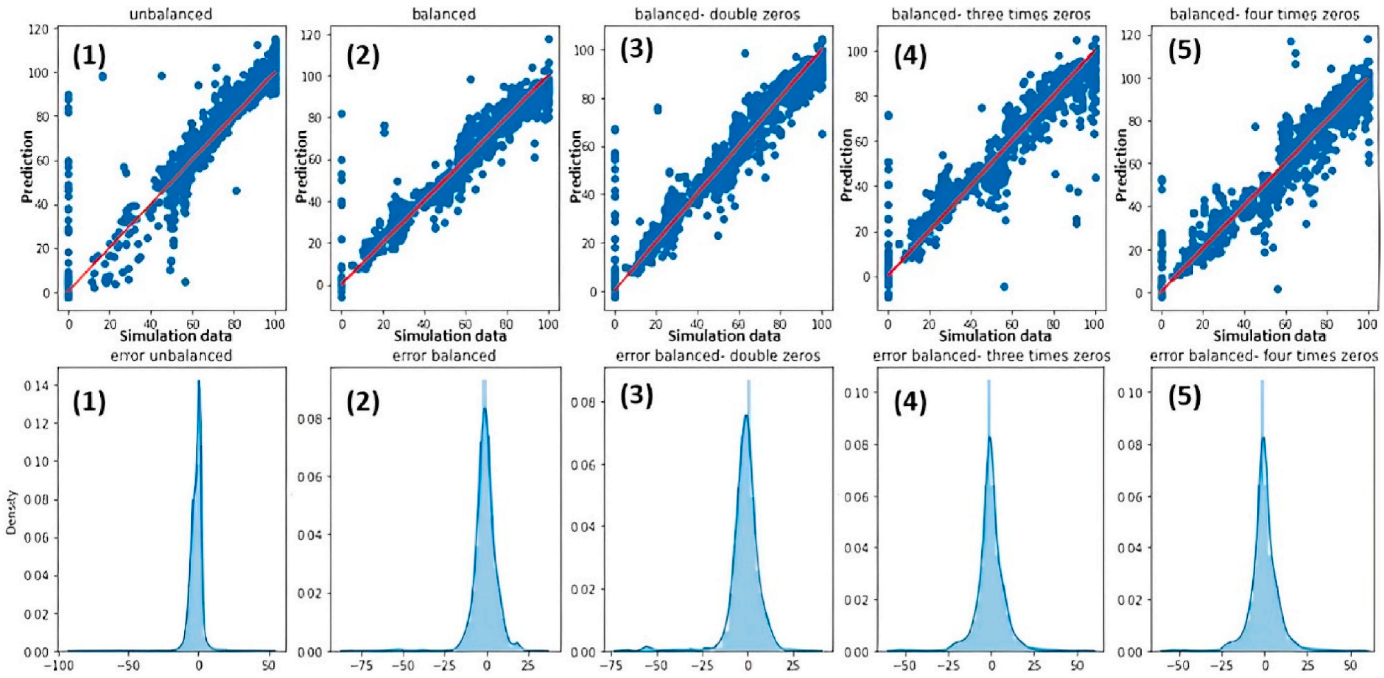


**Fig. 17.** Scatter plot (simulated vs. predicted) and density plot of error for five datasets in Fig. 12.

**Table 8**
Specifications of the models used in the second step selecting the number of hidden layers and neurons.

| MODEL NUMBER | 1 | 2 | 3 | 4 | 5 | 6 | 7 | 8 |
|---|---|---|---|---|---|---|---|---|
| NO. OF INPUT PARAMETERS | 6 | 6 | 6 | 6 | 6 | 6 | 6 | 6 |
| NO. OF HIDDEN LAYERS | 1 | 2 | 3 | 4 | 5 | 6 | 7 | 8 |
| NO. OF NEURONS | 19 | 19 | 19 | 19 | 19 | 19 | 19 | 19 |
| ACTIVATION FUNCTION | ReLU | ReLU | ReLU | ReLU | ReLU | ReLU | ReLU | ReLU |
| TRAINING ALGORITHM | Adam | Adam | Adam | Adam | Adam | Adam | Adam | Adam |
| LEARNING RATE | 0.001 | 0.001 | 0.001 | 0.001 | 0.001 | 0.001 | 0.001 | 0.001 |

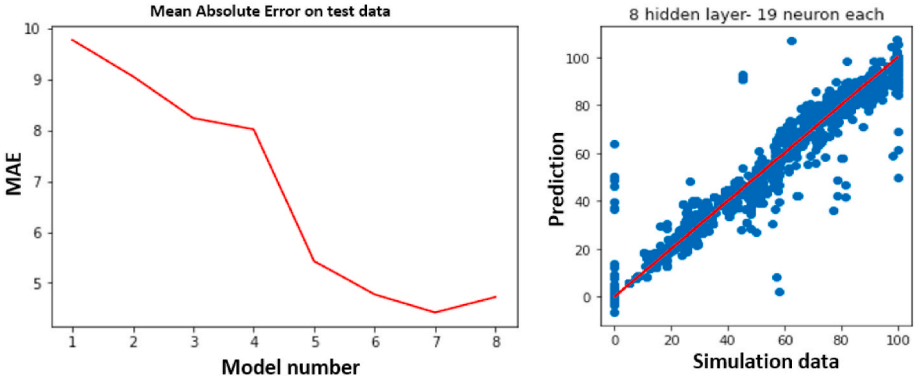


**Fig. 18.** MAE for models in Table 8 and scatter plot for selected model (no. 7).

**Table 9**
Specifications of the models used in the first step selecting the number of hidden layers and neurons.

| MODEL NUMBER | 1 | 2 | 3 | 4 | 5 | 6 | 7 | 8 | 9 | 10 | 11 | 12 |
|---|---|---|---|---|---|---|---|---|---|---|---|---|
| NO. OF INPUT PARAMETERS | 6 | 6 | 6 | 6 | 6 | 6 | 6 | 6 | 6 | 6 | 6 | 6 |
| NO. OF HIDDEN LAYERS | 7 | 7 | 7 | 7 | 7 | 7 | 7 | 7 | 7 | 7 | 7 | 7 |
| NO. OF NEURONS | 19 | 19 | 19 | 19 | 19 | 19 | 19 | 19 | 19 | 19 | 19 | 19 |
| ACTIVATION FUNCTION | ReLU | ReLU | ReLU | ReLU | ReLU | ReLU | ReLU | ReLU | ReLU | Relu | Relu | Relu |
| TRAINING ALGORITHM | Adam | Adam | Adam | Adam | Adam | Adam | Adam | Adam | Adam | Adam | Adam | Adam |
| LEARNING RATE | 0.00025 | 0.0003 | 0.00035 | 0.0004 | 0.00045 | 0.0005 | 0.0007 | 0.001 | 0.003 | 0.005 | 0.007 | 0.01 |

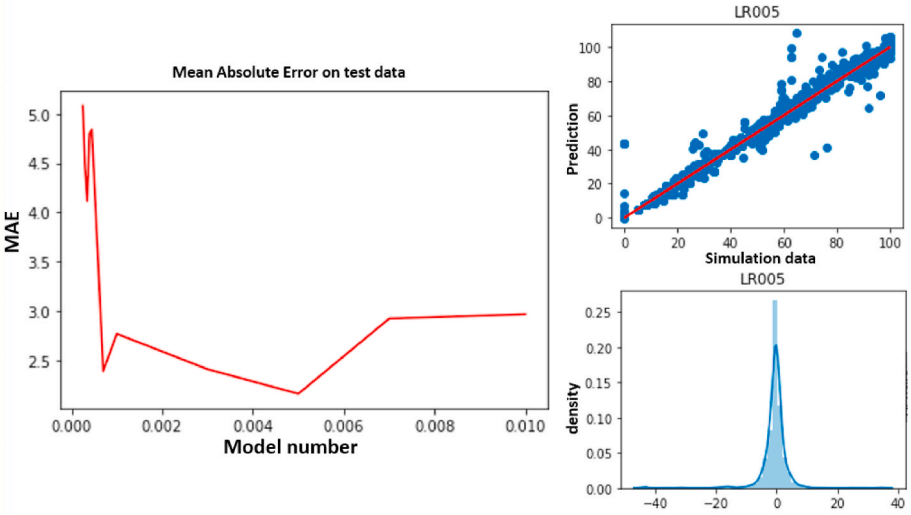


**Fig. 19.** MAE for different learning rates for ANNs in Table 7 and scatter plot and density plot for model no. 10 (selected model).

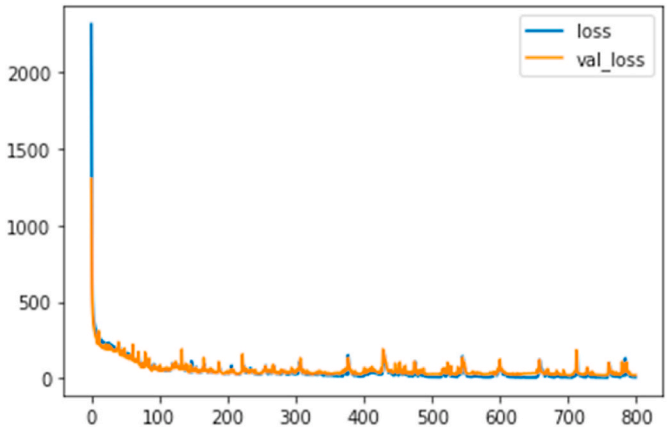


**Fig. 20.** Evolution of the loss and the validation loss over the epochs for the final model.

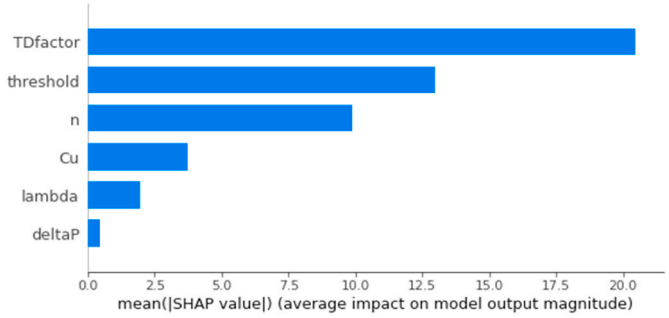


**Fig. 21.** Bar plot of absolute value for average SHAP value for each feature in the selected model.

be optimized and train ANNs with different learning rates, as shown in Table 9. It can be seen in Fig. 19, model no. 10, with a value of 0.005 for the learning rate, has a minimum MAE. Also, the density plot of this model is normal, and its scatter plot shows that it could successfully capture the behavior of cases with zero permeability reduction.

#### 4.2.8. Model assessment

In previous steps, the main purpose was to select the best ANN for predicting the permeability reduction due to polymer gel injection. Fig. 20 shows the loss and validation loss plot during the training step in 800 epochs. It can be seen that the model completely captured the behavior of the data. Validation loss behaves exactly like the loss function, meaning there was no over-fitting during the training step.

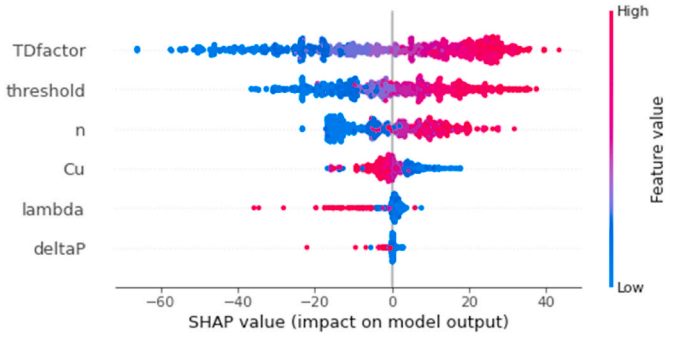


**Fig. 22.** Beeswarm summary plot for the SHAP value.

While the primary goal of this research was to achieve the best accuracy in predicting the target parameter, further analysis of the model using the SHAP library could be considered as another useful step. A bar plot indicating the importance and contribution of parameters in training the model is shown in Fig. 21. In the vertical axis, features are ordered from the highest to the lowest effect on the prediction. As expected, gelation parameters, i.e., TDfactor and Threshold, had the most crucial roles in training the model. The next important feature also was the power-law index (n) which indicates the shear-dependency of fluid.

Fig. 22 shows the beeswarm summary plot for the selected model to go deeper in the analysis. The horizontal axis indicates how much the features contributed to predicting output via SHAP value. As stated in the color bar, the color of the points indicates the value of the data. The higher values contributed to increasing the predicted value for the top three most critical features, i.e., TDfactor, Threshold, and n. On the other hand, reverse behavior is seen for the other three parameters.

## 5. Conclusion

This paper proposes a novel approach for calculating the permeability reduction in a 2D Berea sample due to polymer gel injection which can be considered as a starting point to complete a research gap in this field. The methodology for this purpose consists of two main parts:

numerical simulation and building ANN. Since validating the result is a crucial part of every numerical study, two validation parts (Poiseuille flow and Darcy flow) are done to ensure that the model can perfectly capture the behavior of non-Newtonian fluid flow in porous media. Then the complexity related to time-dependency of the fluid, the model is used to conduct more than 20,000 simulations by varying the input parameters, which provided us with a big dataset. Doing several steps of data cleaning, balancing dataset, and HPO, our final network could capture the permeability changes with less than 2% MAE.

The results of this paper could be briefly summarized below.

1 In the numerical simulation part, it can be seen that gels were mostly formed in larger pores, which is desirable for water shutoff operations in oil and gas reservoirs. The proposed model could successfully capture the behavior of flowing polymer gel fluid in porous media and the changes in pore structure resulting from injecting this fluid.
2 Since the numerical simulation is used to generate our dataset, precise DOE was necessary to ensure that the final network could capture the wide range of behavior for polymer gel injection in porous media.
3 Because the generated dataset was highly unbalanced, balancing this dataset was the primary and most crucial step in constructing a reliable ANN. It could be seen that networks that were trained with an unbalanced dataset had a poor prediction for estimating permeability changes near zero. The process of balancing the dataset of this research was one of the innovative part of that. The steps which were discussed can be used for any regression problem.
4 Model assessment with SHAP in the final stage of this research shows that gelation parameters, i.e., TDfactor and Threshold were the most critical parameters in the learning process, and the power-law index is the next important one.

## Credit author statement

**Elahe Kamel Targhi (Eli):** Conceptualization, Methodology, Software, Coding, Investigation, Writing Original Draft, Formal Analysis; **Mohammad Emami Niri:** Conceptualization, Validation, Resources, Supervision, Writing Review & Editing; **Pacelli L. J. Zitha**: Validation, Supervision, Writing Review & Editing.

## Declaration of competing interest

The authors declare that they have no known competing financial interests or personal relationships that could have appeared to influence the work reported in this paper.

## Data availability

Codes this research is publicly available in the GitHub repository of the first author. Numerical simulation: https://github.com/kamelelahe/NN-LBM.git Machine learning: https://github.com/kamelelahe/ML-NN-LBM.git

## Acknowledgement

we have no known competing financial interests or personal relationships that could have appeared to influence the work reported in this paper.

## References

Alajmi M, Ertekin T. The development of an artificial neural network as a pressure transient analysis tool for applications in double-porosity reservoirs. InAsia Pacific oil and gas conference and exhibition 2007 Oct 30. OnePetro.

Al-Kaabi, A.U., Lee, W.J., 1993. Using artificial neural networks to identify the well test interpretation model (includes associated papers 28151 and 28165). SPE Form. Eval. 8 (3), 233–240.

Al-Shajalee, F., Arif, M., Machale, J., Verrall, M., Almobarak, M., Iglauer, S., Wood, C., 2020. A multiscale investigation of cross-linked polymer gel injection in sandstone gas reservoirs: implications for water shutoff treatment. Energy Fuels 34 (11), 14046–14057.

Anbar, S., Thompson, K.E., Tyagi, M., 2019. The impact of compaction and sand migration on permeability and non-Darcy coefficient from pore-scale simulations. Transport Porous Media 127 (2), 247–267.

Ashrafizaadeh, M., Bakhshaei, H., 2009. A comparison of non-Newtonian models for lattice Boltzmann blood flow simulations. Comput. Math. Appl. 58 (5), 1045–1054.

Bai, B., Zhou, J., Yin, M., 2015a. A comprehensive review of polyacrylamide polymer gels for conformance control. Petrol. Explor. Dev. 42 (4), 525–532.

Bai, B., Zhou, J., Yin, M., 2015b. A comprehensive review of polyacrylamide polymer gels for conformance control. Petrol. Explor. Dev. 42 (4), 525–532.

Bhatnagar, P.L., Gross, E.P., Krook, M., 1954. A model for collision processes in gases. I. Small amplitude processes in charged and neutral one-component systems. Phys. Rev. 94 (3), 511.

Boek, E.S., Venturoli, M., 2010. Lattice-Boltzmann studies of fluid flow in porous media with realistic rock geometries. Comput. Math. Appl. 59 (7), 2305–2314.

Boyd, J., Buick, J.M., 2007. Comparison of Newtonian and non-Newtonian flows in a two-dimensional carotid artery model using the lattice Boltzmann method. Phys. Med. Biol. 52 (20), 6215.

Da Wang Y, Armstrong RT, Mostaghimi P. Enhancing resolution of digital rock images with super resolution convolutional neural networks. Journal of Petroleum Science and Engineering. 2019 Nov 1;182:106261.

Dong, L., Yue, X., Su, Q., Qin, W., Song, W., Zhang, D., Zhang, Y., 2016. Study on the plugging ability of polymer gel particle for the profile control in reservoir. J. Dispersion Sci. Technol. 37 (1), 34–40.

Gokhale, M.Y., Fernandes, I., 2017. Simulation of forced convection in non-Newtonian fluid through sandstones. Int. J. Comput. Methods Eng. Sci. Mech. 18 (6), 302–308.

Golparvar, A., Zhou, Y., Wu, K., Ma, J., Yu, Z., 2018. A comprehensive review of pore scale modeling methodologies for multiphase flow in porous media. Advances in Geo-Energy Research 2 (4), 418–440.

Haddadpour, H., Emami Niri, M., 2021. Uncertainty assessment in reservoir performance prediction using a two-stage clustering approach: proof of concept and field application. J. Petrol. Sci. Eng. 204, 108765 https://doi.org/10.1016/J.PETROL.2021.108765.

Haghshenas, Y., Emami Niri, M., Amini, S., Amiri Kolajoobi, R., 2020. Developing grid-based smart proxy model to evaluate various water flooding injection scenarios. Petrol. Sci. Technol. 38 (17), 870–881. https://doi.org/10.1080/10916466.2020.1796703.

Haghshenas, Y., Niri, M.E., Amini, S., Kolajoobi, R.A., 2021. A physically-supported data-driven proxy modeling based on machine learning classification methods: application to water front movement prediction. J. Petrol. Sci. Eng. 196, 107828 https://doi.org/10.1016/J.PETROL.2020.107828.

Hennigh O. Lat-net: compressing lattice Boltzmann flow simulations using deep neural networks. arXiv preprint arXiv:1705.09036. 2017 May 25.

Jia, H., Pu, W.-F., Zhao, J.-Z., Liao, R., 2011. Experimental investigation of the novel phenol– formaldehyde cross-linking HPAM gel system: based on the secondary cross-linking method of organic cross-linkers and its gelation performance study after flowing through porous media. Energy Fuels 25 (2), 727–736.

Jiasheng, L.I.U., 2013. Improvement and test of water plugging technology for horizontal wells in heavy oil reservoirs with edge and bottom water. Contemp. Chem. Ind. 42 (3), 290–293.

Kamrava S, Tahmasebi P, Sahimi M. Enhancing images of shale formations by a hybrid stochastic and deep learning algorithm. Neural Networks. 2019 Oct 1;118:310-20.

Kehrwald, D., 2005. Lattice Boltzmann simulation of shear-thinning fluids. J. Stat. Phys. 121 (1), 223–237.

Kolajoobi, R.A., Niri, M.E., Amini, S., Haghshenas, Y., 2023. A data-driven proxy modeling approach adapted to well placement optimization problem. Journal of Energy Resources Technology, Transactions of the ASME 145 (1). https://doi.org/10.1115/1.4055908/1147343.

Kolajoobi, R., Haddadpour, H., Niri, M.E., 2021. Investigating the capability of data-driven proxy models as solution for reservoir geological uncertainty quantification. J. Petrol. Sci. Eng. 205, 108860.

Lashari ZA, Memon A, Ansari U, Memon HU, Tunio AH. Simulating the Effects of Water Shut-off Treatment by Polymer Gel Injection. InPAPG/SPE Pakistan section Annual Technical Conference 2014 Nov 24. OnePetro.

Latt, J., Malaspinas, O., Kontaxakis, D., Parmigiani, A., Lagrava, D., Brogi, F., Belgacem, M. Ben, Thorimbert, Y., Leclaire, S., Li, S., 2021. Palabos: parallel lattice Boltzmann solver. Comput. Math. Appl. 81, 334–350.

Le, T., Vo, M.T., Vo, B., Lee, M.Y., Baik, S.W., 2019. A hybrid approach using oversampling technique and cost-sensitive learning for bankruptcy prediction. Complexity 2019.

Liao, J., 2014. Gel Treatment Field Application Survey for Water Shut off in Production Wells.

Lundberg, S.M., Lee, S.-I., 2017. A unified approach to interpreting model predictions. Adv. Neural Inf. Process. Syst. 30.

Malaspinas, O., Courbebaisse, G., Deville, M., 2007. Simulation of generalized Newtonian fluids with the lattice Boltzmann method. Int. J. Mod. Phys. C 18 (12), 1939–1949.

Martys, N.S., Chen, H., 1996. Simulation of multicomponent fluids in complex three-dimensional geometries by the lattice Boltzmann method. Phys. Rev. 53 (1), 743.

Masroor, M., Emami Niri, M., Rajabi-Ghozloo, A.H., Sharifinasab, M.H., Sajjadi, M., 2022. Application of machine and deep learning techniques to estimate NMR-derived permeability from conventional well logs and artificial 2D feature maps. J. Pet. Explor. Prod. Technol. https://doi.org/10.1007/S13202-022-01492-3.

Mohaghegh, S., Ameri, S., 1995. Artificial Neural Network as a Valuable Tool for Petroleum Engineers. Paper SPE, p. 29220.
Mohaghegh, S., Ameri, S., Arefi, R., 1996. Virtual measurement of heterogeneous formation permeability using geophysical well log responses. Log. Anal. 37 (2), 32–39.
Nikravesh, M., Kovscek, A.R., Johnston, R.M., Patzek, T.W., 1996. Prediction of Formation Damage during Fluid Injection into Fractured, Low Permeability Reservoirs via Neural Networks. SPE Formation Damage Control Symposium.
Ohta, M., Toyooka, T., Matsukuma, Y., 2020. Numerical simulations of Carreau-model fluid flows past a circular cylinder. Asia Pac. J. Chem. Eng. 15 (6), e2527.
Olson, J.F., Rothman, D.H., 1997. Two-fluid flow in sedimentary rock: simulation, transport and complexity. J. Fluid Mech. 341, 343–370.
Parmigiani, A., Huber, C., Bachmann, O., Chopard, B., 2011. Pore-scale mass and reactant transport in multiphase porous media flows. J. Fluid Mech. 686, 40–76.
Rabault, J., Kuchta, M., Jensen, A., Réglade, U., Cerardi, N., 2019. Artificial neural networks trained through deep reinforcement learning discover control strategies for active flow control. J. Fluid Mech. 865, 281–302. https://doi.org/10.1017/JFM.2019.62.
Rahimi, M., Abbaspour-Fard, M.H., Rohani, A., 2021. Machine learning approaches to rediscovery and optimization of hydrogen storage on porous bio-derived carbon. J. Clean. Prod. 329, 129714 https://doi.org/10.1016/J.JCLEPRO.2021.129714.
Sen, M., Yang, K.T., 2008. A review of multiphase flow and Heat transfer with artificial neural networks. American Society of Mechanical Engineers, Heat Transfer Division, (Publication) HTD 374 (4), 79–86. https://doi.org/10.1115/IMECE2003-41761.
Shahkarami, A., Mohaghegh, S., Gholami, V., Haghighat, A., Moreno, D., 2014. Modeling pressure and saturation distribution in a CO2 storage project using a Surrogate Reservoir Model (SRM). Greenhouse Gases: Sci. Technol. 4 (3), 289–315.
Sharifinasab, M.H., Emami Niri, M., Masroor, M., 2023. Developing GAN-boosted Artificial Neural Networks to model the rate of drilling bit penetration. Appl. Soft Comput. 136, 110067 https://doi.org/10.1016/J.ASOC.2023.110067.
Sukop, M.C., Huang, H., Lin, C.L., Deo, M.D., Oh, K., Miller, J.D., 2008. Distribution of multiphase fluids in porous media: comparison between lattice Boltzmann modeling and micro-x-ray tomography. Phys. Rev. 77 (2), 26710.
Sutera, S.P., Skalak, R., 1993. The history of Poiseuille's law. Annu. Rev. Fluid Mech. 25 (1), 1–20.
Sydansk, R.D., Romero-Zerón, L., 2011. Reservoir Conformance Improvement. Society of Petroleum Engineers Richardson, TX.
Taha, A., Amani, M., 2019. Overview of water shutoff operations in oil and gas wells; chemical and mechanical solutions. ChemEngineering 3 (2), 51.
Tahmasebi, P., Kamrava, S., Bai, T., Sahimi, M., 2020. Machine learning in geo-and environmental sciences: from small to large scale. Adv. Water Resour. 142, 103619.
Van Si, L., Chon, B.H., 2018. Effective prediction and management of a CO2 flooding process for enhancing oil recovery using artificial neural networks. Journal of Energy Resources Technology, Transactions of the ASME 140 (3). https://doi.org/10.1115/1.4038054/442916.
Veliyev, E.F., Aliyev, A.A., Guliyev, V.V., Naghiyeva, N.V., 2019. Water shutoff using crosslinked polymer gels. In: SPE Annual Caspian Technical Conference.
Vo Thanh, H., Sugai, Y., Sasaki, K., 2020. Application of artificial neural network for predicting the performance of CO2 enhanced oil recovery and storage in residual oil zones. Sci. Rep. 10 (1), 1–16. https://doi.org/10.1038/s41598-020-73931-2, 2020 10:1.
Wang, C.-H., Ho, J.-R., 2011. A lattice Boltzmann approach for the non-Newtonian effect in the blood flow. Comput. Math. Appl. 62 (1), 75–86.
Wang, D., Bernsdorf, J., 2009. Lattice Boltzmann simulation of steady non-Newtonian blood flow in a 3D generic stenosis case. Comput. Math. Appl. 58 (5), 1030–1034.
Yoshino, M., Hotta, Y., Hirozane, T., Endo, M., 2007. A numerical method for incompressible non-Newtonian fluid flows based on the lattice Boltzmann method. J. Non-Newtonian Fluid Mech. 147 (1–2), 69–78.
Zheng, J., Wang, Z., Ju, Y., Tian, Y., Jin, Y., Chang, W., 2021. Visualization of water channeling and displacement diversion by polymer gel treatment in 3D printed heterogeneous porous media. J. Petrol. Sci. Eng. 198, 108238.
Zitha, P.L.J., Botermans, C.W., Hoek, J. vd, Vermolen, F.J., 2002. Control of flow through porous media using polymer gels. J. Appl. Phys. 92 (2), 1143–1153.
Zou Q, He X. On pressure and velocity flow boundary conditions for the lattice Boltzmann BGK model. arXiv preprint comp-gas/9508001. 1995 Aug 8.